ORIGINAL PAPER

The quantification of low-probability–high-consequences events: part I. A generic multi-risk approach

Arnaud Mignan · Stefan Wiemer · Domenico Giardini

Abstract Dynamic risk processes, which involve interactions at the hazard and risk levels, have yet to be clearly understood and properly integrated into probabilistic risk assessment. While much attention has been given to this aspect lately, most studies remain limited to a small number of site-specific multi-risk scenarios. We present a generic probabilistic framework based on the sequential Monte Carlo Method to implement coinciding events and triggered chains of events (using a variant of a Markov chain), as well as time-variant vulnerability and exposure. We consider generic perils based on analogies with real ones, natural and man-made. Each simulated time series corresponds to one risk scenario, and the analysis of multiple time series allows for the probabilistic assessment of losses and for the recognition of more or less probable risk paths, including extremes or low-probability–high-consequences chains of events. We find that extreme events can be captured by adding more knowledge on potential interaction processes using in a brick-by-brick approach. We introduce the concept of risk migration matrix to evaluate how multi-risk participates to the emergence of extremes, and we show that risk migration (i.e., clustering of losses) and risk amplification (i.e., loss amplification at higher losses) are the two main causes for their occurrence.

Keywords Multi-hazard · Multi-risk · Extreme event · Monte Carlo · Markov chain

1 Introduction

Multi-risk assessment is still in its infancy and often only refers to the analysis of multiple single hazards in a same framework (Grünthal et al. 2006; Carpignano et al. 2009; Schmidt

A. Mignan (✉) · S. Wiemer
Swiss Seismological Service, ETH Zurich, Zurich, Switzerland
e-mail: arnaud.mignan@sed.ethz.ch

A. Mignan · D. Giardini
Institute of Geophysics, ETH Zurich, Zurich, Switzerland

et al. 2011). Major catastrophes however remind us that multi-risk is not simply the sum of individual risks but that correlations between natural hazards, technological hazards and our complex socioeconomic networks lead to greater risks (e.g., 2005 hurricane Katrina, USA; 2010 eruption of Eyjafjallajökull, Iceland; 2011 Tohoku earthquake, Japan). Innovative methods have been proposed in recent years to tackle the problem of hazard interactions (e.g., Marzocchi et al. 2012) and of other dynamic aspects of risk, such as time-dependent vulnerability and exposure (e.g., Selva 2013) or network failures (e.g., Adachi and Ellingwood 2008). However, so far, only a limited number of scenario-based and/or site-specific multi-risk studies have been proposed due to the difficulty and novelty of the task.

Development of a comprehensive multi-risk framework is hampered by the following requirements: (1) large amount of input data (2) cross-disciplinary expertise and (3) innovative risk assessment methods. The first two points are generally solved in dedicated multi-risk projects at the national (e.g., HAZUS-MH, http://www.fema.gov/hazus), international (e.g., CAPRA, http://www.ecapra.org/) or private sector levels (e.g., Grossi and Kunreuther 2005; Schmidt et al. 2011). The third point remains to be solved. As indicated by Kappes et al. (2012), "despite growing awareness of relations between hazards, still neither a uniform conceptual approach nor a generally used terminology is applied". Similarly, but based on feedback from civil protection stakeholders, Komendantova et al. (2014) noted that: "two areas are most problematic. These are (1) the absence of clear definitions and (2) the lack of information on the added value of multi-risk assessment".

In the present study, we present a novel, generic, multi-risk framework based on the sequential Monte Carlo Method (MCM) to allow for a straightforward and flexible implementation of hazard interactions, which may occur in a complex system. Real-world examples of hazard interactions include: earthquake clustering, storm clustering, tsunamis following earthquakes or landslides, landslides or fire following earthquakes, storm surges associated to hurricanes, technological accidents triggered by natural events (i.e., NaTech events). Time-variant vulnerability and exposure related to hazard clustering are also considered, although not the primary focus of this study. More generally, time-variant vulnerability may refer to different processes, such as structure ageing, not-repaired pre-damage due to past events or damage conditioned on the co-occurrence of several events. Time-variant exposure supposes the evolution of assets value with time, which may be due to socioeconomic factors or to previous losses.

Our goal is specifically to capture and quantify extreme (i.e., low-probability–high-consequences) events using inductive generalization (e.g., Bier et al. 1999) and by following the recommendation of Kameda (2012), which is to "mobilize "scientific imagination" in the process of decision"—by incorporating extreme events in risk modelling if no observations but sound scientific bases are available (Note that the term "reasoned imagination" is used by Paté-Cornell 2012). Our approach differs from site-specific and scenario-based studies (e.g., Adachi and Ellingwood 2008; Marzocchi et al. 2012; Selva 2013) in that we do not define any specific hazard or risk interaction but a framework to implement any type of interaction. With such an objective, real interaction processes have to be abstracted to more basic concepts and engineering methods by-passed. The proposed framework is described in Sect. 2, in which the concept of hazard correlation matrix is introduced.

Validation of our framework, which should be considered as a proof-of-concept, is made using generic data and processes defined heuristically. This strategy, that is the use of intuitive judgment and simple rules, allows for the solving of problems that are

otherwise difficult to consider. Based on an extensive literature survey, we generalize the concepts of peril, of peril characterization and of hazard interaction. Our aim, by abstracting these concepts into basic categories, is to provide some general guidelines for extreme event quantification. The proof-of-concept is presented in Sect. 3, and a discussion on the applicability of the proposed framework to real-world conditions is given in Sect. 4.

Basic hazard and risk terms as well as definitions used in the present article are based, when available, on the book "Catastrophe Modelling: A new approach to managing risk" by Grossi and Kunreuther (2005). Symbols used in our study are listed in Table 1.

2 Generic multi-risk framework

2.1 Sequential Monte Carlo Method

The proposed multi-risk framework is formed of a core simulation algorithm based on the MCM. We adopt the MCM for its flexibility when dealing with complex systems. We generate N_{sim} time series, sampling events from a Poisson distribution (homogeneous or non-homogeneous process). Each time series represents one risk scenario, and the analysis

Table 1 List of the symbols used in the present study

| Symbols	Description
$A, B, C, \ldots$	Peril identifier
$A_i, B_i, C_i, \ldots$	Stochastic event identifier
i, j, k	Increment
n	Number of events
N_{sim}	Number of simulations
t	Time in the interval $\Delta t = [t_0; t_{max}]$
ε	Time lapse between two correlated events ($\varepsilon \ll \Delta t$)
λ	Long-term occurrence rate
λ_{mem}	Time-variant occurrence rate
β	Event frequency–intensity ratio
ι	Hazard intensity
δ	Mean damage ratio (i.e., system damage)
μ	Mean of lognormal vulnerability curve
σ	Standard deviation of lognormal vulnerability curve
γ	Calibration factor for conditional vulnerability curve
Λ	System loss
E	System exposure
e	Reconstruction function
$\Pr(j|i)$	Probability of occurrence of event j conditional on event i
α	Shape parameter of the lognormal distribution for event repeat
ΔT_{ij}	Time shift in occurrence rate of event j due to event i
f	Coupling factor
ϕ	Index of dispersion

of N scenarios allows for the probabilistic assessment of losses and for the recognition of more or less probable risk paths. These risk paths emerge naturally from the system implemented in the MCM.

A set of stochastic events is defined as input for the MCM, with each event characterized by an identifier, a long-term occurrence rate λ and a loss Λ. The loss is defined as $\Lambda = \delta\, E$ with δ the mean damage ratio and E the system exposure. δ is derived from the hazard intensity ι with each event being represented by one unique hazard footprint. Each event is therefore implicitly related to one specific source, e.g., an earthquake related to a given fault segment, a storm related to a given track (see Sect. 3.1.1 for the definition of a stochastic event set).

Hazard interactions as well as time-variant exposure and vulnerability represent non-stationary processes, which require additional inputs (see Sects. 3.1.2, 3.1.3) and a sequential processing strategy. The proposed sequential MCM is defined as follows:

- *Multi-hazard assessment:* define the simulation set with simulation identifier, event identifier and event occurrence time t.

    1. Generate N_{sim} random time series: Sample N_{sim} sets of events over the time interval $\Delta t = [t_0;\ t_{\max}]$ drawn from the Poisson distribution with each stochastic event i characterized by the long-term rate parameters λ_i. Affix an occurrence time t to each event following the random uniform distribution. Record the time series in the simulation set S_0, which represents the null hypothesis H_0 of having no interaction in the system. Fix increment $j = 1$, which indicates the occurrence of the first event in the time series.
    2. For each of the N_{sim} simulations, record the characteristics of the jth event, which occurs at t_j, in simulation set S_1. Resample events k occurring in the interval $[t_j;\ t_{\max}]$ if the conditional probability $\Pr(k|j)$ exists. This conditional probability is defined in the hazard correlation matrix, described in Sect. 2.2. Affix $t_k = t_j + \varepsilon$ with $\varepsilon \ll \Delta t$. Fix $j = j + 1$.
    3. Repeat step 2 while $t_j \leq t_{\max}$.
    4. Fix $j = 1$.

- *Multi-risk assessment:* update the simulation sets S_0 and S_1 with event loss Λ.

    5. For each of the N_{sim} simulations, calculate the mean damage ratio δ_j due to the jth event, which is potentially conditional on the occurrence of previous events. The implementation of time-variant vulnerability is described in Sect. 2.3.
    6. For each of the N_{sim} simulations, calculate the loss Λ_j due to the jth event, which is potentially conditional on the occurrence of previous events. The implementation of time-variant exposure is also described in Sect. 2.3. Record Λ_j.
    7. Repeat steps 5 and 6 while $t_j \leq t_{\max}$.

Figure 1a illustrates the difference between simulation sets S_0 and S_1. All simulated time series in S_1 start with the same event as in S_0, since changes are only conditional on the occurrence of previous events. Following an event, changes may or may not occur in S_1 depending on the conditional probabilities and the effects of sampling. Once an event is triggered, the trigger/target pair clusters in time with chains of n events potentially emerging in the time interval $[t,\ t + n\varepsilon]$. The impact of time-variant exposure and vulnerability on event losses are not represented in Fig. 1a. It should be noted that the proposed framework for hazard interactions is a variant of a Markov chain. In that view,
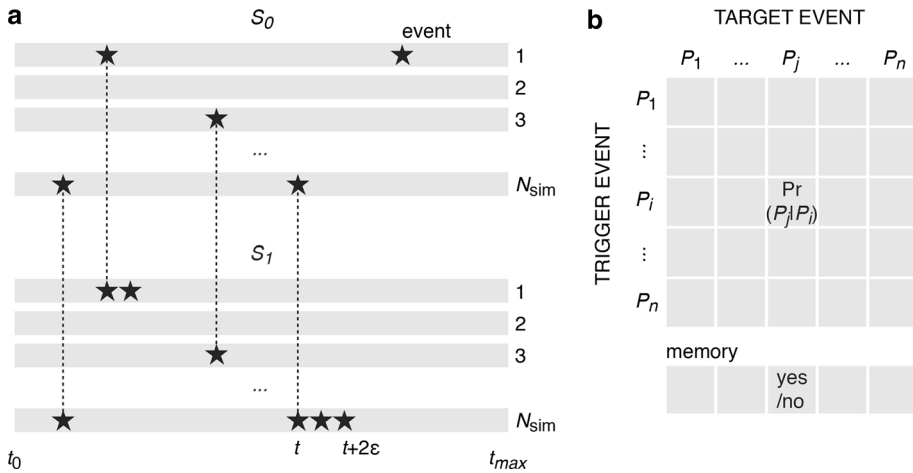
Fig. 1 Generic multi-risk framework (multi-hazard part). **a** Sequential MCM: the simulation set S_0 represents the null hypothesis H_0 of having no interaction in the system, while set S_1 represents any multi-risk hypothesis. *Grey rectangles* represent different simulated time series. **b** Concept of hazard correlation matrix: trigger events are represented in rows i and target/triggered events in columns j. A given peril P consists of n events P_i with $1 \leq i \leq n$. Each cell of the square matrix indicates the 1-to-1 conditional probability of occurrence $\Pr(P_j|P_i)$ over Δt, which is used as input in the MCM. The n-to-1 conditional probability is considered by incorporating a memory element to the correlation matrix. The proposed approach can be seen as a variant of a Markov chain. See text for details

the hazard correlation matrix corresponds to a transition matrix, the conditional probabilities to transition probabilities and events to states.

2.2 Hazard correlation matrix

We introduce the concept of hazard correlation matrix to quantify hazard interactions. It should be noted that we use a loose definition of the word interaction, as we also refer to one-way causal effects by this term (noted→). The hazard correlation matrix is illustrated in Fig. 1b where trigger events are represented in rows i and target/triggered events in columns j. A given peril P consists of n events P_i with $1 \leq i \leq n$. Each cell of the square matrix indicates the 1-to-1 conditional probability of occurrence $\Pr(j|i) = \Pr(P_j|P_i)$ over Δt, which is used as input in the MCM. We also consider the n-to-1 conditional probability by incorporating a memory element to the correlation matrix. Various interaction processes may be implemented, based on empirical, statistical or physical laws. Those are run in the background with only the conditional probability represented in the hazard correlation matrix. However, the memory element is defined such that it can alter the process in the background by informing it of the sequence of previous events. This is illustrated by several examples in Sect. 3.1.2. The approach is different from a strict Markov chain in the fact that it is not memoryless and because the matrix does not require $\sum_j \Pr(j|i) = 1$ (i.e., finite chains of events).

We define various terms (noted in *italics*) to categorize different types of interactions based on the concept of hazard correlation matrix: An *event repeat* is described by $P_i \rightarrow P_i$, an *intra-hazard interaction* by $P_i \rightarrow P_j$ and an *inter-hazard interaction* by $A_i \rightarrow B_j$ with A and B two different perils. Moreover, perils can be separated into *primary*

perils A when $\lambda_A > 0$ and *secondary perils B* when $\lambda_B = 0$ and $\Pr(B|A) > 0$, with λ the long-term occurrence rate. *Invisible events i*, which do not yield direct losses, should be included in the system if they trigger events j that do (case $\Pr(j|i) > 0$, $\Lambda_i = 0$ and $\Lambda_j > 0$).

2.3 Time-variant exposure and time-variant vulnerability

Cumulative losses due to the occurrence of successive events cannot exceed the total exposure E. Time-variant exposure can be defined by.

$$E_i = E_0 - \sum_{i=1}^{i} \delta_i E_{i-1} + e_i \tag{1}$$

where E_0 the original exposure, E_i the exposure of the system immediately following event i and e_i a function representing the exposure reconstruction up to the occurrence time of event i. With a time-variant exposure, the event loss also becomes time-variant with $\Lambda_i = \delta_i E_{i-1}$. Two end-members of Eq. 1 are instantaneous reconstruction (i.e., $e_i = \sum \Lambda_i$) with $E_i = E_0$ and no reconstruction (i.e., $e_i = 0$) with $0 \leq E_i \leq E_0$. Both cases are tested in Sect. 3. Although not considered in the present study, a time-dependent term $e(t)$ could be added to Eq. 1 to represent system recovery after a disaster and socioeconomic evolution (e.g., increase in wealth/assets with time).

The clustering of events in time may also influence the vulnerability, which can be described by the conditional mean damage ratio $\delta_{j|i}$. The dependence on the trigger event i may take different forms, independently of the framework developed here. An example of vulnerability dependence on hazard intensity is given in Sect. 3.1.3. Time-dependent vulnerability $\delta_i(t)$, such as ageing, is not considered.

3 Proof-of-concept

3.1 Generic data and processes

We generate generic data and processes by following the heuristic method and by abstracting the concepts of peril, of peril characterization and of hazard interaction into basic categories. Our approach provides some general guidelines for extreme event quantification and a dataset for testing the generic multi-risk framework described in Sect. 2. It follows the existing recommendations on extreme event assessment (Bier et al. 1999; Kameda 2012; Paté-Cornell 2012) by combining inductive generalization and "scientific imagination" to include known examples of extremes as well as potential "surprise" events in a same framework. We intentionally do not consider the case of networks (Adachi and Ellingwood 2008). Data and processes are then implemented in the MCM, and the results analysed in Sects. 3.2 and 3.3. In the present study, we use $N_{\text{sim}} = 10^5$, $\Delta t = [t_0 = 0; t_{\max} = 1]$ and $\varepsilon = 0.01$. It should be noted that the numerous assumptions made below are not a requirement of the proposed multi-risk framework but are working hypotheses for basic testing purposes.

3.1.1 Building a stochastic event set

We first generate a stochastic event set in which each event is defined by an identifier, a long-term occurrence rate λ and a loss Λ. Let's consider peril A consisting of n_A events A_i with $1 \leq i \leq n_A$. First, we define the frequency-intensity distribution

$$\lambda_i = \exp(-\beta \iota_i) \tag{2}$$

where ι_i is the hazard intensity of event A_i, λ_i the long-term occurrence rate of event A_i and β the exponential law exponent for peril A. Equation 2 applies to numerous perils, such as earthquakes (Gutenberg and Richter 1944), volcanic eruptions (Simkin and Siebert 1994) or asteroid impacts (Brown et al. 2002). Second, we estimate the mean damage ratio δ of repair cost to the replacement cost of the system from a vulnerability curve that relates the susceptibility of the system to the hazard intensity, with 0 (no damage) $\leq \delta \leq 1$ (total destruction). We use the cumulative lognormal distribution

$$\delta_i = \frac{1}{2} erfc \left(-\frac{\ln(\iota_i) - \mu}{\sigma\sqrt{2}} \right) \tag{3}$$

where ι_i is the hazard intensity and δ_i the mean damage ratio due to event A_i. μ and σ are, respectively, the mean and standard deviation of the variable's logarithm and depend on the peril and asset response type (see Sect. 3.1.3 for a variable μ). Equation 3 is well suited to describe the typical S-shaped vulnerability curve used in damage assessment for earthquakes (Fabbrocino et al. 2005), volcanic eruptions (Spence et al. 2005; Zuccaro et al. 2008), winds (Wehner et al. 2010), fluvial floods (Reese and Ramsay 2010), tsunamis (Srivihok et al. 2012) or asteroid impacts (Mignan et al. 2011). In the present case, we consider a single-damage state, which is an oversimplification compared to standard risk assessment. This limitation is discussed in Sect. 4.

Let's now consider additional perils other than A. Direct comparison of hazards (so-called joint visualization of multiple hazards) would require the use of a rather subjective hazard intensity classification scheme (e.g., low–medium–high) (Kappes et al. 2012) since intensity ι differs from one peril to another one (e.g., ground shaking, ash load, inundation depth, wind speed, bolide energy). Thus, we remove ι by combining Eqs. 2 and 3, which yields

$$\delta_i = \frac{1}{2} erfc \left(-\frac{\ln(-\ln(\lambda_i)) - \ln(\beta) - \mu}{\sigma\sqrt{2}} \right) \tag{4}$$

Using risk as a common language, we resolve the problem of hazard comparability. Event loss Λ_i is then defined by $\Lambda_i = \delta_i E$ where $E = 1$ the system exposure. Since a unique vulnerability curve is used for the full exposure, all losses given in the present study are mean loss values.

We generate the stochastic event set based on Eq. 4 with $10^{-4} \leq \lambda_i \leq 10^{-1}$ in 0.1 increments in the log scale. It follows that 31 events are defined per peril with return periods varying from 10 to 10,000 years. This applies only to primary perils (here A and B), which occur spontaneously following Eq. 2. We fix $\beta_A = \ln(10)$ and $\beta_B = 0.5\ln(10)$ (Fig. 2a). Perils A and B are analogue to earthquakes and volcanic eruptions for instance. Secondary perils (here C, D and E), by definition, have a null long-term occurrence rate $\lambda = 0$ and only occur following primary events. Examples include tsunamis following earthquakes (Suppasri et al. 2012), storm surges (Irish et al. 2008) or Natech events (i.e., industrial accidents with natural hazard triggers, Krausmann et al. 2011). Vulnerability curve parameters (Eq. 3, Fig. 2b) are fixed such that perils A and B show distinctive risks (i.e., different risk ranking), with peril A dominating risk at short return periods and peril B dominating risk at long return periods (Eq. 4, Fig. 2c). We use $\mu_A = \ln(5)$, $\sigma_A = 0.4$, $\mu_B = \ln(6)$ and $\sigma_B = 0.1$. We define three events per secondary peril (C_1–C_3, D_1–D_3 and E_1–E_3) and use a same vulnerability step function such that $\delta_1 = 0.01$, $\delta_2 = 0.1$ and $\delta_3 = 1$ for the 3 perils. Table 2 shows the resulting stochastic event set, which is used as input in the MCM.
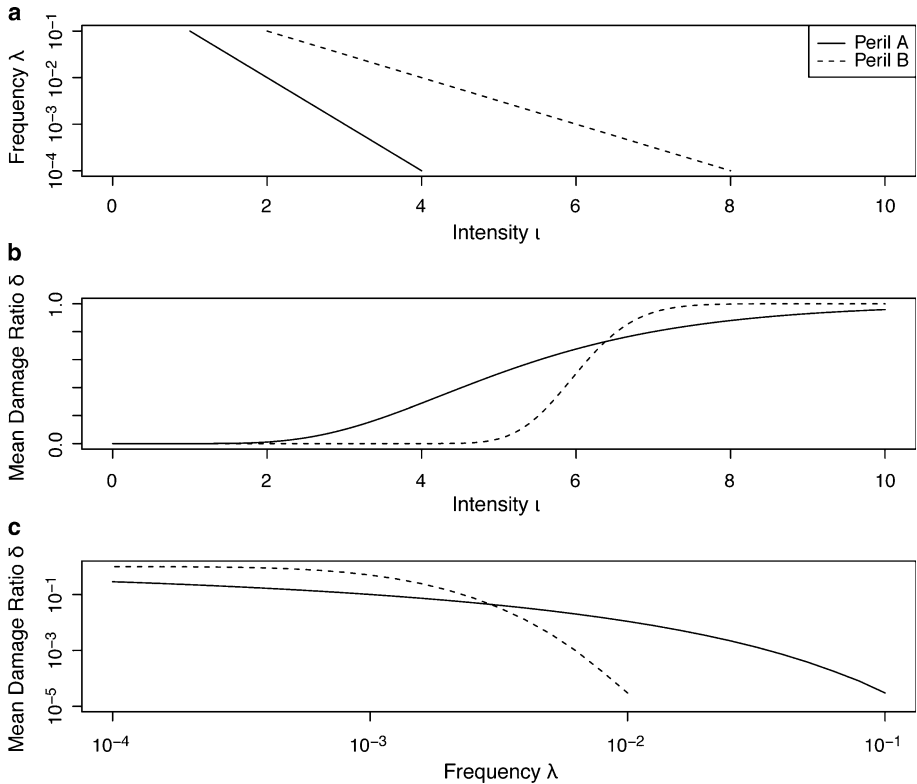
Fig. 2 Characteristics of the generic primary perils *A* and *B*. **a** Power-law frequency–intensity distributions with frequency λ and intensity ι (Eq. 2). **b** Cumulative lognormal vulnerability curves defined by the mean damage ratio δ as a function of intensity ι (Eq. 3). **c.** Risk curves defined by the mean damage ratio δ as a function of frequency λ (Eq. 4). The list of parameters is given in Table 3

3.1.2 Populating the hazard correlation matrix

Providing a comprehensive review of hazard interactions is out of the scope of this study. Such a daunting task was for example described by Gill and Malamud (2012) (see also Kappes et al. 2012). Here, we describe the principal types of hazard interactions that can be implemented in the correlation matrix to be used for proof-of-concept of the proposed multi-risk framework. The proposed hazard correlation matrix is shown in Fig. 3. We consider the three categories of interactions previously defined: event repeat (e.g., $A_i \rightarrow A_i$; $C \rightarrow C$), intra-hazard interaction (e.g., $A_i \rightarrow A_j$) and inter-hazard interaction (e.g., $A_i \rightarrow B_j$). The effect can be positive (i.e., probability increase) or negative (i.e., probability decrease),, and temporary or lasting (concept of memory). Table 3 lists the different combinations defined in Fig. 3 and examples of analogies with real perils. More types of interactions could be envisioned, as not all possible combinations are described here (primary vs. secondary/interaction category/effect/memory or not).
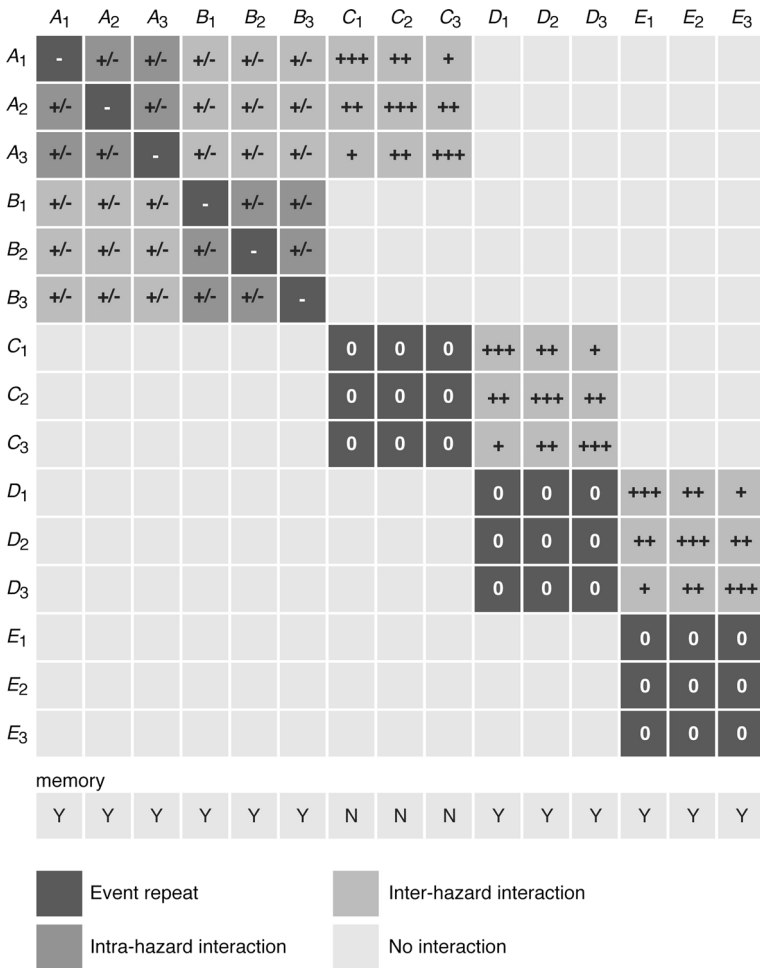
Event repeat for primary perils is here described by the lognormal distribution

Table 2 Stochastic event set defined as input for the MCM

Event id.	λ	Λ	Event id.	λ	Λ
A_1	0.100000	0.00003	B_6	0.031623	0
A_2	0.079433	0.00008	B_7	0.025119	0
A_3	0.063096	0.00018	B_8	0.019953	0
A_4	0.050119	0.00038	B_9	0.015849	0
A_5	0.039811	0.00073	B_{10}	0.012589	0
A_6	0.031623	0.00131	B_{11}	0.010000	0.00003
A_7	0.025119	0.00220	B_{12}	0.007943	0.00018
A_8	0.019953	0.00350	B_{13}	0.006310	0.00096
A_9	0.015849	0.00532	B_{14}	0.005012	0.00394
A_{10}	0.012589	0.00778	B_{15}	0.003981	0.01283
A_{11}	0.010000	0.01099	B_{16}	0.003162	0.03415
A_{12}	0.007943	0.01505	B_{17}	0.002512	0.07620
A_{13}	0.006310	0.02006	B_{18}	0.001995	0.14608
A_{14}	0.005012	0.02611	B_{19}	0.001585	0.24509
A_{15}	0.003981	0.03326	B_{20}	0.001259	0.36727
A_{16}	0.003162	0.04156	B_{21}	0.001000	0.50000
A_{17}	0.002512	0.05104	B_{22}	0.000794	0.62872
A_{18}	0.001995	0.06173	B_{23}	0.000631	0.74063
A_{19}	0.001585	0.07359	B_{24}	0.000501	0.82986
A_{20}	0.001259	0.08662	B_{25}	0.000398	0.89471
A_{21}	0.001000	0.10079	B_{26}	0.000316	0.93851
A_{22}	0.000794	0.11605	B_{27}	0.000251	0.96593
A_{23}	0.000631	0.13227	B_{28}	0.000200	0.98189
A_{24}	0.000501	0.14948	B_{29}	0.000158	0.99104
A_{25}	0.000398	0.16751	B_{30}	0.000126	0.99564
A_{26}	0.000316	0.18634	B_{31}	0.000100	0.99799
A_{27}	0.000251	0.20581	C_1	0	0.01
A_{28}	0.000200	0.22559	C_2	0	0.1
A_{29}	0.000158	0.24661	C_3	0	1
A_{30}	0.000126	0.26717	D_1	0	0.01
A_{31}	0.000100	0.28847	D_2	0	0.1
B_1	0.100000	0	D_3	0	1
B_2	0.079433	0	E_1	0	0.01
B_3	0.063096	0	E_2	0	0.1
B_4	0.050119	0	E_3	0	1
B_5	0.039811	0			

Each event is defined by its identifier, long-term occurrence rate λ (relative to Δt) and expected loss Λ. Values for primary perils (A and B) are obtained from Eq. 4. Secondary perils (C, D and E) have a long-term rate $\lambda = 0$ by definition. The system exposure is fixed to $E = 1$

	A_1	A_2	A_3	B_1	B_2	B_3	C_1	C_2	C_3	D_1	D_2	D_3	E_1	E_2	E_3
A_1	-	+/-	+/-	+/-	+/-	+/-	+++	++	+						
A_2	+/-	-	+/-	+/-	+/-	+/-	++	+++	++						
A_3	+/-	+/-	-	+/-	+/-	+/-	+	++	+++						
B_1	+/-	+/-	+/-	-	+/-	+/-									
B_2	+/-	+/-	+/-	+/-	-	+/-									
B_3	+/-	+/-	+/-	+/-	+/-	-									
C_1							0	0	0	+++	++	+			
C_2							0	0	0	++	+++	++			
C_3							0	0	0	+	++	+++			
D_1										0	0	0	+++	++	+
D_2										0	0	0	++	+++	++
D_3										0	0	0	+	++	+++
E_1													0	0	0
E_2													0	0	0
E_3													0	0	0

memory

Y	Y	Y	Y	Y	Y	N	N	N	Y	Y	Y	Y	Y	Y

■ Event repeat   ■ Inter-hazard interaction

■ Intra-hazard interaction   ■ No interaction

Fig. 3 Hazard correlation matrix with examples of potential interactions. Trigger events are represented in rows i and target/triggered events in columns j. Each cell indicates the 1-to-1 conditional probability of occurrence $\Pr(j|i)$ over Δt. The n-to-1 conditional probability is considered by incorporating a memory element to the correlation matrix. See Table 3 for an analogy with real perils and real interaction processes

$$\Pr(A_i|A_i) = \int_{t_0}^{t_{\max}} \frac{1}{t\sqrt{2\pi\alpha_i^2}} \exp\left(-\frac{(\ln(t) - 1/\lambda_i)^2}{2\alpha_i^2}\right) dt \tag{5}$$

where λ_i is the long-term occurrence rate of event A_i and $\alpha_i = 1$ the shape. In Eq. 5, the probability over Δt is very low immediately following t_0 for $\Delta t \ll 1/\lambda_i$ and progressively increases through time. It hence represents a renewal process in which energy is first released by an event and then accumulates gradually through time due to a loading process. It applies for example to earthquakes, which occurrence is controlled by tectonic loading (Parsons 2005). We apply Eq. 5 to perils A and B, which significantly lowers the probability of occurrence compared to the long-term probability $\Pr(A_i) = 1 - \exp(-\lambda_i \Delta t)$ for $\Delta t \ll 1/\lambda_i$ (Fig. 4). Event repeat for secondary perils is described by

Table 3 Characteristics of generic perils and processes and analogy with real ones

Peril	Type	Parameters	Analogy
A	Primary	$\beta_A = \ln(10)$, $\mu_A = \ln(5)$, $\sigma_A = 0.4$	E.g., earthquake
B		$\beta_B = 0.5\ln(10)$, $\mu_B = \ln(6)$, $\sigma_B = 0.1$	E.g., volcanic eruption
C	Secondary	$\delta_1 = 0.01$, $\delta_2 = 0.1$, $\delta_3 = 1$	E.g., tsunami
D			E.g., Natech (i.e., technological accident with natural hazard trigger)
E			E.g., technological accident

Category	Effect	Memory	Parameters	Analogy
Repeat	Pr ↓	Yes	$\alpha = 1$	E.g., earthquake on same fault
Repeat	Pr = 0	Yes	–	E.g., technological accident on same non-repaired infrastructure impossible
Repeat	Pr = 0	No	–	E.g., second tsunami after same earthquake impossible
Intra-hazard	Pr ↑↓	Yes	$f = 0.1$	E.g., earthquakes on different faults
Inter-hazard	Pr ↑↓	Yes		E.g., volcanic eruption → earthquake
Inter-hazard	Pr ↑	Yes	–	E.g., → technological accident only if infrastructure still functional
Inter-hazard	Pr ↑	No	–	E.g., earthquake → tsunami; hurricane → storm surge

The different combinations correspond to the ones defined in the hazard correlation matrix shown in Fig. 3

$Pr(C_j|C_i) = Pr(D_j|D_i) = Pr(E_j|E_i) = 0$, which indicates that a given peril can only occur once, whether immediately after the event (case of peril C—no memory) or through Δt (case of perils D and E—with memory) (Fig. 3; Table 3). Peril C is analogue to a tsunami or storm surge, which can occur anytime the proper trigger occurs, but only once per triggering. Perils D and E are analogue to technological accidents. If such an accident yields non-functionality, the same accident cannot occur again if the critical infrastructure is not repaired. If it were repaired immediately, it would then be in the peril C class (Table 3). Memory is here defined by the recording of previous instances of event occurrences.

We consider that primary perils are due to an underlying loading process, as described previously for repeating events by Eq. 5. In this case, events are advanced or delayed from a time shift ΔT_{ij}. We define

$$Pr(j|i) = 1 - \exp(-\lambda_{j,\text{mem}}\Delta t) \text{ for } i \neq j \tag{6}$$

based on the non-homogenous Poisson process with i the trigger event, j the target event and

$$\lambda_{j,\text{mem(updated)}} = \frac{1}{1/\lambda_{j,\text{mem}} + \Delta T_{ij}} \tag{7}$$

$\Delta T_{ij} > 0$ represents a time delay. $\lambda_{j,\text{mem}}$ is updated after each event occurrence j, including the case $i = j$, and represents the memory of the process (at t_0, $\lambda_{j,\text{mem}} = \lambda_j$). The same
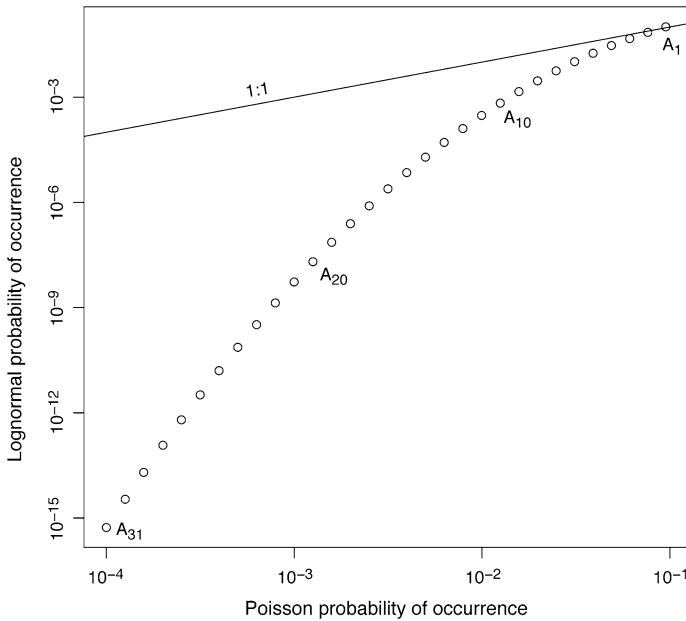
Fig. 4 Probability of occurrence $\Pr(A_i|A_i)$ of a repeating event based on the lognormal probability distribution (Eq. 5) compared to the Poisson probability distribution

approach is used in earthquake interaction modelling, which is well established with the theory of stress transfer (Toda et al. 1998; King 2007). This theory also applies to earthquake/volcanic eruption interactions (Hill et al. 2002; Eggert and Walter 2009). Here, we apply Eqs. 6 and 7 to intra-hazard interactions ($A_i \rightarrow A_j$; $B_i \rightarrow B_j$) and to inter-hazard interactions ($A_i \rightarrow B_j$; $B_i \rightarrow A_j$) (Fig. 2). We define the matrix $\Delta T_{ij} = \pm f/\lambda_i$ where f an ad hoc coupling factor, such that the time shift due to event i is proportional to the return period of this event (i.e., a rare large event will have a greater effect than a small, more common, event). Since the spatial relationship between different events is not considered, we simply fix the sign of ΔT_{ij} randomly for each target event j. We fix $f = 0.1$ (the role of different values is discussed in Sect. 3.3).

Secondary perils occur based on the following one-way causal effects: $A \rightarrow C$, $C \rightarrow D$ and $D \rightarrow E$ (Fig. 3). Hence, we can produce the domino effect $A \rightarrow C \rightarrow D \rightarrow E$. We consider a linear relationship between trigger event i and target event j, such that

$$j(i) = \frac{n_j - 1}{n_i - 1}(i - 1) + 1 \tag{8}$$

where n_i and n_j are the number of stochastic events i and j, respectively. This is described in Fig. 5a for the cases $A \rightarrow C$ and $C \rightarrow D$ (same for $D \rightarrow E$). It shows that for any event i, in the range $[1, n_i]$, there is an associated event j in the range $[1, n_j]$. Using a relationship between event increments is however artificial. For real perils, the relationship would normally relate hazard intensities ι_i to ι_j. Examples include the relationship $h = 3.10^{-5}M^{6.2344}$ between tsunami height h and earthquake magnitude M (Suppasri et al. 2012) or the relationship between storm surge height and maximum wind speed, as defined in the Saffir–Simpson hurricane scale (e.g., Irish et al. 2008). Such simple relationships are
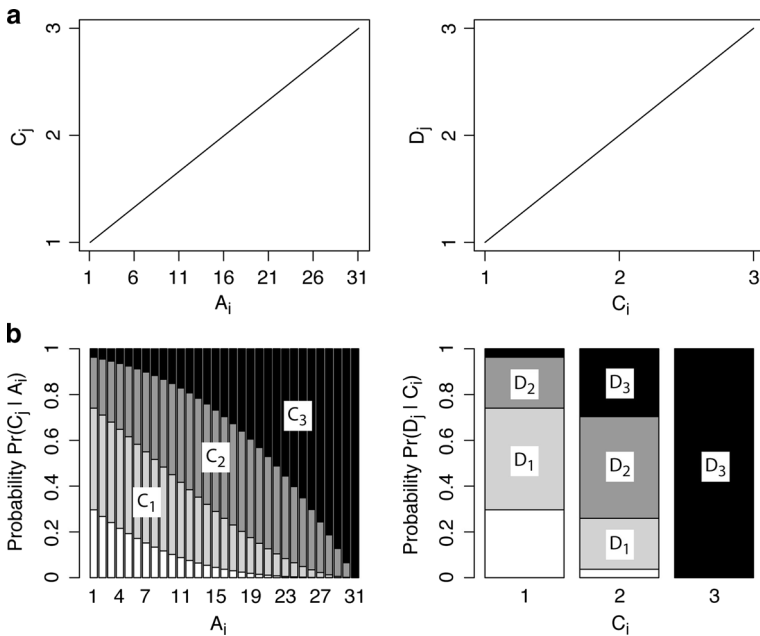
Fig. 5 Conditional probability of occurrence of secondary perils Pr($C|A$) and Pr($D|C$). **a** Ad hoc linear relationship between trigger increment i and target increment j (i.e., proxy to hazard intensity, Eq. 8). **b** Conditional probabilities defined from a binomial distribution (Eq. 9) based on Eq. 8. See text for details

controversial, since effects depend on site conditions. The concepts remain however valid at a more abstract level. In the generic case presented here, we relate event increments directly for sake of simplicity. To determine the conditional probability Pr($j|i$), we assume a binomial distribution

$$\Pr(k|i) = \frac{n_j!}{k!(n_j - k)!}\left(\frac{j(i)}{n_j}\right)^k \left(1 - \frac{j(i)}{n_j}\right)^{n_j - k} \tag{9}$$

where $0 \leq k \leq n_j$. $k = j$ except for the case $k = 0$, which corresponds to the probability of having no event triggered Pr($\emptyset|i$). Pr($k|i$) is shown in Fig. 5b. Note that the higher the trigger increment i is (i.e., proxy to hazard intensity), the greater is the probability of triggering a severe target event j; which is a direct consequence of Eq. 8.

3.1.3 Considering time-variant vulnerability

Hazard clustering may also influence the vulnerability of the system. One example, which has recently been considered, is the increase in vulnerability to ground shaking due to increased structural load following an ash fall (Zuccaro et al. 2008; Selva 2013). Another well-known case is the increased vulnerability of structures to successive shakings during an earthquake cluster (Jalayer et al. 2010). Here, we consider the conditional vulnerability curve
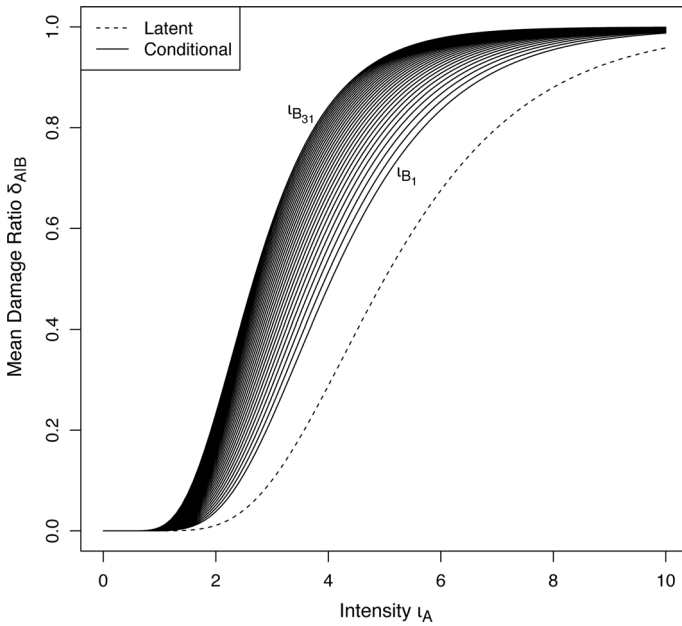
Fig. 6 Vulnerability curve of peril *A* conditional on the occurrence of peril *B*. The curve shifts to higher damage for a same hazard intensity ι_A with the intensity ι_B increasing (Eq. 10)

$$\delta_{j|i} = \frac{1}{2} erfc \left(-\frac{\ln\left(\iota_j\right) - \mu_{j|i}}{\sigma_j\sqrt{2}} \right) \qquad (10)$$

where $\delta_{j|i}$ the mean damage ratio due to event *j* conditional on the occurrence of event *i* and $\mu_{j|i} = \mu_j - \gamma\ln(\iota_i)$. ι_i and ι_j are the hazard intensities of events *i* and *j*, respectively, and γ is an ad hoc calibration parameter. The proposed generic relationship is based on the idea that the higher the intensity ι_i is, the greater is the vulnerability to event *j*. The validity of such formulation remains to be verified with the logarithmic term here only proposed for consistency within Eq. 10. For real data, a different relationship may be obtained empirically or from structural engineering (Zuccaro et al. 2008; Jalayer et al. 2010). Here, we apply Eq. 10 to perils *A* and *B* for the case $\delta_{A|B}$ where $\gamma = 0.3$. Figure 6 shows the vulnerability curve linked to peril *A* conditional on the occurrence of events B_1 to B_{31}. This process is analogue to increased vulnerability to earthquake shaking due to the occurrence of a volcanic eruption with ash fall (Zuccaro et al. 2008; Selva 2013).

3.2 Definition of extremes

Extreme events may be defined as events, which are "rare, severe and outside the normal range of experience of the system in question" (Bier et al. 1999). This definition however assumes that extreme events are somewhat anomalous. In this line of reasoning, quantification of extremes would make them normal, i.e., non-extreme. In the present study, extreme events are simply defined as low-probability–high-consequences events, whether they seem normal or abnormal. Here, extremes do not only refer to individual events, but also to groups of events of which only the overall impact is considered. Therefore, the

definition of an event remains blurry and depends on the level considered in the system (i.e., an event may be composed of sub-events and a meta-event of events). Then, extremes are categorized into individual events (Sect. 3.2.1) and multiple events, i.e., coinciding events or triggered chains of events (Sect. 3.2.2).

In recent years, anomalous events, or outliers, have been repackaged into fancier animals, some of which made their way into popular culture. Taleb (2007) coined the term "black swan" to describe rare events, which in principle cannot be anticipated. Another popular term is "perfect storm", which refers to an event resulting of a rare combination of circumstances (Paté-Cornell, 2012). Finally, the concept of "dragon king" introduced by Sornette and Ouillon (2012) explains that outliers are due to a physical mechanism not represented in the distribution tail considered. These different terms are not used in the present study.

3.2.1 Individual extreme events: concept of heavy tail

Let's first consider the role of individual events on the overall risk. Figure 7 shows the metric $\lambda_i \Lambda_i$. (loss over Δt) for events i characterized by their long-term occurrence rate λ_i and loss Λ_i (Table 2). A related metric is the annual average loss (AAL). As described in Sect. 3.1.1, peril A dominates the risk at higher frequencies, while peril B dominates at lower frequencies. The highest loss over period Δt is due to event A_{15} (at $\lambda = 0.0039$) for peril A and to event B_{21} (at $\lambda = 0.0010$) for peril B. We see that although we consider most of the risk in our stochastic event set, we miss a non-negligible part below $\lambda = 10^{-4}$. It is common practice in insurance industry to only consider risk scenarios with a return period that does not exceed 1,000 years (Smolka 2006). In our example and with $\Delta t = 1$ year, we would miss most of the risk using such an arbitrary choice (grey area in Fig. 7). This illustrates the concept of heavy tail from which extremes are populated. This tail is however bounded whether by the maximum possible event size (e.g., concept of earthquake maximum magnitude in seismic hazard assessment) or by the exposure (i.e., loss saturation).

Rare unknown perils could also contribute to overall risk, showing the potential instability of the risk process, as any added information on possible extreme events could significantly, if not dramatically, alter the risk measure (Fig. 7). The level of knowledge on extreme individual events is directly linked to the length of the available records (Smolka 2006). New approaches, such as the study of myths (Piccardi and Masse 2007) or of odd geomorphological structures (e.g., Scheffers et al. 2012) within the scope of scientific imagination, should help improving these records and reassess the overall risk. This is however out of the scope of the present study.

3.2.2 Coinciding events and triggered chains of events

Implementation and evaluation of coinciding events and triggered chains of events is the main purpose of this work. Coinciding events are independent events, which occur in cluster by chance. Such behaviour is in principle trivial to treat (if all events are known—see previous section), since it emerges naturally from the Poisson process. This is illustrated in Fig. 8 where the distribution of the number of event occurrences k per simulation for simulation set S_0 (homogeneous Poisson process, null hypothesis H_0) is shown in light grey. With the event rate $\lambda_{tot} = \sum \lambda = 0.97$ (Table 2), we find for instance that the probability of having $k = 5$ events occurring during the same simulation is $\Pr(k = 5) \sim 0.003$. Large sets of coinciding events are however controlled by the
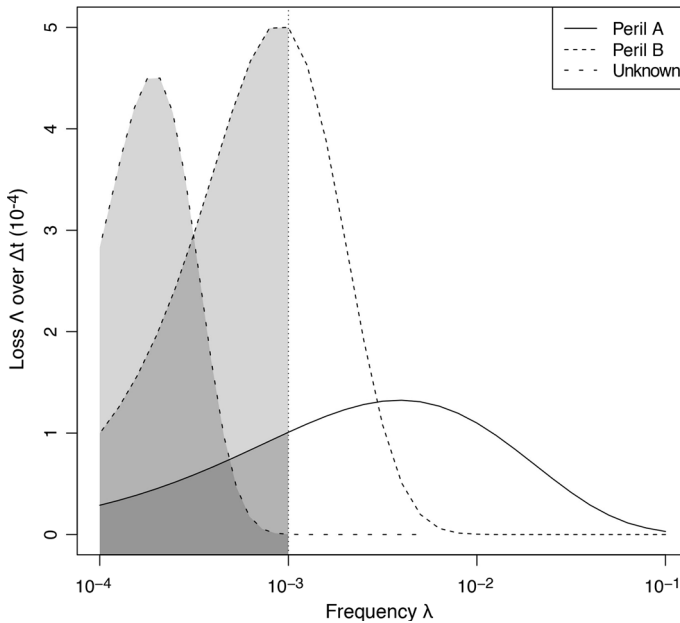
Fig. 7 Metric $\lambda_i \Lambda_i$ (loss over Δt) for events i characterized by their long-term occurrence rate λ_i and loss Λ_i (Table 2). Using an arbitrary minimum rate in risk assessment, e.g., $\lambda \geq 10^{-3}$, may yield an underestimation of the risk. Rare unknown perils could also contribute to overall risk, showing the potential instability of the risk process, as any added information on possible extreme events could significantly, if not dramatically, alter the risk measure. Here, an ad hoc $\lambda_i \Lambda_i$ distribution is shown to illustrate the potential role of an unknown peril

moderate-size events with low return periods. More damaging events are rarer and their random co-occurrence even rarer.

Chains of events are the result of interaction processes. This means that their clustering is non-random. Here we consider chains of events by adding knowledge to the system by implementing the generic interaction processes described in Sects. 2.2 (hazard contribution) and 2.3 (risk contribution). We test four different hypotheses H_1 to H_4 (four simulation sets S_1 to S_4), as defined in Table 4. These what-if scenarios are as follows: primary peril interactions between events of type A and B (H_1); primary peril interactions and time-variant vulnerability linked to the clustering of events of type A and B (H_2); primary and secondary peril interactions (including $A \rightarrow C \rightarrow D \rightarrow E$ chains) and time-variant vulnerability (H_3); and finally, primary and secondary peril interactions, time-variant vulnerability and time-variant exposure (i.e., no reconstruction) (H_4). All these hypotheses are based on the data and processes defined in Sect. 3.1. Results are discussed below.

3.3 Emergence of extremes

3.3.1 Risk migration

In hypothesis H_1, events from perils A and B interact following the rules described previously (Fig. 3; Eqs. 6–7). The number of events per simulation is compared to the one expected in the null hypothesis H_0 in Fig. 8. Using the akaike information criterion (AIC), we find that the number of event occurrences k per simulation for simulation set S_1 (in dark
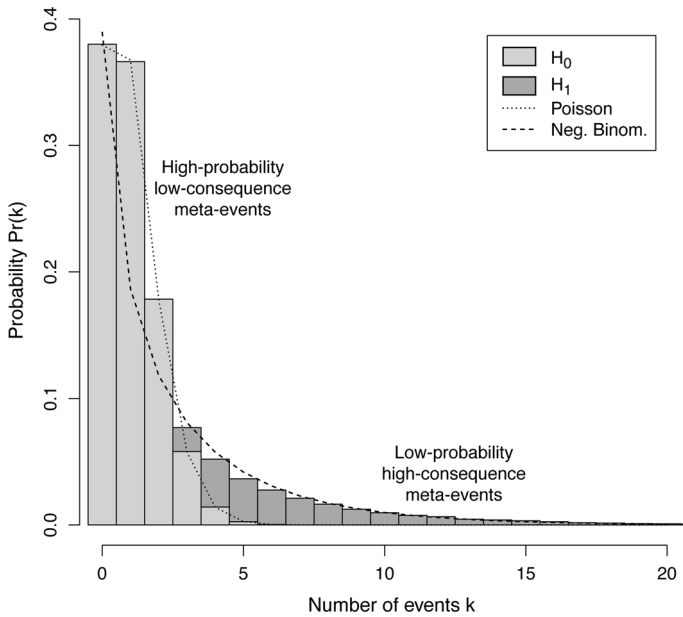
Fig. 8 Probability distribution of the number of events k per simulation showing the migration of risk to lower-probability–higher-consequences meta-events when hazard interactions are considered. Definition of hypotheses H_0 and H_1 is given in Table 4

Table 4 List of tested hypotheses H

H	Primary peril interactions	Secondary peril interactions	Time-variant vulnerability	Time-variant exposure
H_0	✗	✗	✗	✗
H_1	✔	✗	✗	✗
H_2	✔	✗	✔	✗
H_3	✔	✔	✔	✗
H_4	✔	✔	✔	✔

grey) is better described by the negative binomial distribution than by the Poisson distribution, which indicates over-dispersion (i.e., clustering of events). Here, we use a coupling factor $f = 0.1$ (see Sect. 3.1.2 for the definition of f), which gives the index of dispersion (variance/mean ratio) $\phi = 4.7$. $0 < \phi < 1$ represents under-dispersion and $\phi > 1$ over-dispersion. A higher f yields a higher ϕ, more coupling yielding more clustering. Let's note that one could directly simulate risk scenarios by sampling from the negative binomial distribution instead of from the Poisson distribution in step 1 of the MCM and by not applying steps 2–3 (see Sect. 2.1). This approach applies when clustering is not due to event interactions but to a higher-level process. The negative binomial distribution is frequently used in storm modelling for instance (Mailier et al. 2006; Vitolo et al. 2009). This is however not tested in the present study.

In Fig. 8, the probability of having $k = 5$ events is $\Pr(k = 5) \sim 0.04$ in set S_1 in contrast with $\Pr(k = 5) \sim 0.003$ in set S_0. For $k = 7$, $\Pr(k = 7) \sim 0.02$ in set S_1 while
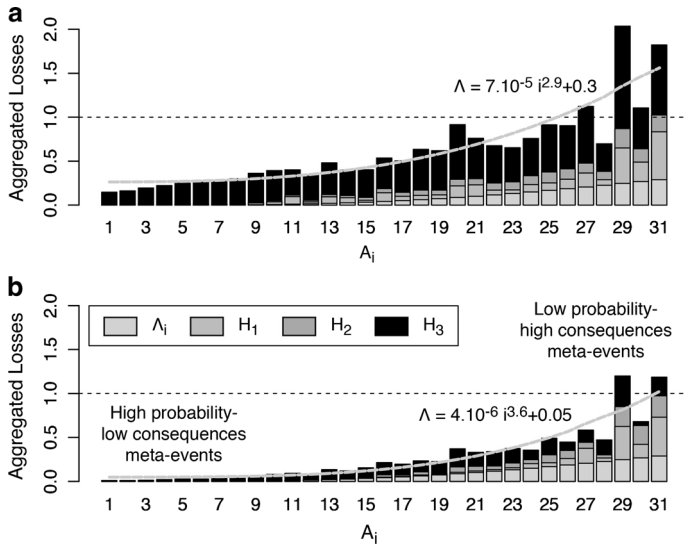
Fig. 9 Aggregated losses as a function of maximum event size A_i showing the amplification of risk at greater risk levels. Definition of hypotheses H_1 to H_3 is given in Table 4. **a** Mean aggregated losses; **b** median aggregated losses

$Pr(k = 7) \sim 0.0004$ in set S_0. With $N_{sim} = 10^5$, we find a maximum number of events per simulation $k_{max} = 7$ in set S_0 and $k_{max} = 41$ in set S_1. For hypothesis H_3, in which the domino effect $A \rightarrow C \rightarrow D \rightarrow E$ is added (Fig. 3), the index of dispersion increases to $\phi = 7.0$, and we get $Pr(k = 5) \sim 0.05$, $Pr(k = 7) \sim 0.03$ and $k_{max} = 49$ in set S_3. This demonstrates that risk migrates to lower-probability–higher-consequences events when hazard interactions are considered. Here, we talk about meta-events, the term consequence being defined as the aggregated loss over the k events of the cluster (assuming in a first time a homogeneous distribution of losses Λ over k).

3.3.2 Risk amplification

As defined in Sect. 3.1.2, the time advance or delay ΔT_{ij} of events j due to a given trigger i increases with the trigger intensity ι (for perils A and B—hypothesis H_1). Therefore, the rarer the event is, the stronger is the associated clustering and the higher is the aggregated loss. Similarly, the higher the intensity ι of a trigger is, the higher is the probability of a larger secondary event (for perils C, D and E; Fig. 5—hypothesis H_3). Finally, the higher the intensity of peril B is, the higher the loss due to peril A is (Fig. 6—hypothesis H_2). This is illustrated in Fig. 9, which shows the mean aggregated losses (Fig. 9a) and the median aggregated losses (Fig. 9b) observed in simulations where the largest event from peril A is A_i. We find that by adding more information on the dynamic risk process, losses tend to be amplified with increasing risk. We can fit the increase in aggregated losses by a power-law relationship with exponent 2.9 and 3.6 for mean and median aggregated losses, respectively. In comparison, the power-law exponent is 2.7 for individual event losses (with $\Lambda_i \sim 3.10^{-5} i^{2.7}$). This indicates a phenomenon of risk amplification for low-probability–high-consequences events.
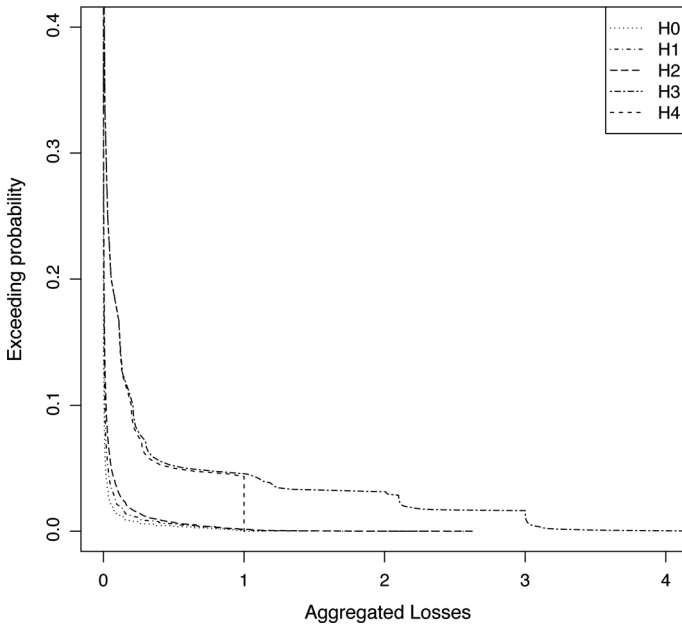
Fig. 10 Exceedance probability (EP) curves for the five hypotheses H_0 to H_4 defined in Table 4

Let's finally remark that aggregated losses saturate to $\sum \Lambda = E_0 = 1$ in hypothesis H_4 if the exposure is not reconstructed after a loss. Moreover, the renewal process of event repeats limits the number of occurrences of any given event (Figs. 3, 4; hypotheses H_1 and H_3). Such processes counteract risk amplification and avoid the emergence of exploding chain reactions. Since the data and processes defined in Sect. 3.1 were carefully selected to be representative of existing perils and interactions based on an extensive survey of the literature, our results (risk migration and amplification) are believed to represent some common characteristics of multi-risk. It is evident that both aspects strongly depend on site conditions and that only the analysis of real sites will permit to determine the real impact of multi-risk. We have demonstrated that the proposed framework could be used for such a task.

3.3.3 A multi-risk metric: the risk migration matrix

We can evaluate the role of multi-risk in the emergence of extremes using two different standard metrics: the exceedance probability (EP) curve (e.g., Grossi et al. 2005; Smolka 2006) and the risk matrix (Cox 1998; Krausmann et al. 2011). Both are different representations of the relationship between event frequency and event loss (in the present study, between frequency of meta-events and aggregated loss). Figure 10 shows EP curves of the five different simulation sets (Table 4). We see the progressive increase in the area below the curve and the tail becoming fatter when more information on the risk process is added. We also see the case of a bounded EP at $\sum \Lambda = E_0 = 1$. However, such a metric provides only limited information on the extreme events that populate the tail of the EP curve.

In contrast, the risk matrix provides a more visual representation of the risk although the colour code, from green (minimum risk) to red (maximum risk) (Krausmann et al. 2011),

remains subjective (Fig. 11, top left). We populate the risk matrix with the risk scenarios or risk paths generated in the different simulation sets. Each simulation is characterized by an aggregated loss, which represents one risk scenario. The number of times N the same aggregated loss is observed gives the frequency N/N_{sim} of this risk scenario. Here, aggregated losses are binned into 0.01 cells in the log scale (i.e., 501 different values in the loss interval $10^{-4} \leq \Lambda \leq 10$). Each risk scenario is then represented by a point in the risk matrix (Fig. 11). Using a smaller bin would shift all values to lower frequencies, but the observed patterns would remain the same. This approach should therefore be considered as semi-quantitative.

To better evaluate the role of multi-risk in the emergence of extremes, we introduce the notion of risk migration matrix, which is shown in Fig. 11. It is defined as the difference in the density of risk scenarios observed between two hypotheses. To avoid a pixellated result, the densities are first calculated using a Gaussian kernel, here with a standard deviation large enough to focus on the first-order migration patterns. The right column shows the case $H_i - H_0$, and the left column shows the case $H_i - H_{i-1}$ with i the hypothesis number (Table 4). Risk scenarios of the first and second hypotheses are represented by white and black points, respectively. An increase in risk is represented in red and a decrease in blue. The proposed approach allows us to visualize how the risk migrates as a function of frequency and aggregated losses when new information is added to the system. From H_0 to H_3, we see a progressive shift of the risk to higher frequencies and higher losses (from yellow to red), indicating that the risk is underestimated when interactions at the hazard and risk levels are not considered. The shift is particularly pronounced in the case of domino effects with $A \rightarrow C \rightarrow D \rightarrow E$. Finally, the risk migration matrix $H_4 - H_3$ shows how time-dependent exposure yields a saturation of losses. Feedback from civil protection stakeholders also showed that a risk matrix view might be preferable to the use of loss curves for communicating multi-risk results. This is in the context of this feedback that the concept of risk migration matrix was developed (Komendantova et al. 2014).

4 Applicability to real-world conditions

We have presented a novel, generic and flexible multi-risk framework, which implements coinciding events, triggered chains of events, time-variant vulnerability and time-variant exposure. While the sequential MCM is a well-established method to model complex systems, it is still rarely used as the basis of a multi-risk assessment tool. Figure 12 shows the difference between standard risk modelling (e.g., Grossi et al. 2005) and the newly proposed approach (Sect. 2). Application of the approach to real test sites will require two improvements: (1) a data switch with the transition from generic to real data and processes, which will be the subject of a companion manuscript by the same authors: "The Quantification of Low-Probability–High-Consequences Events: Part II. Guidelines to Multi-Risk Assessment Based on the Virtual City Concept" and (2) an integration of engineering models that are in use in existing risk tools (e.g., moving from a single-damage state equation (Eq. 3) to more realistic multi-damage states as described for instance in

Standard Risk Modelling

Proposed Multi-Risk Modelling
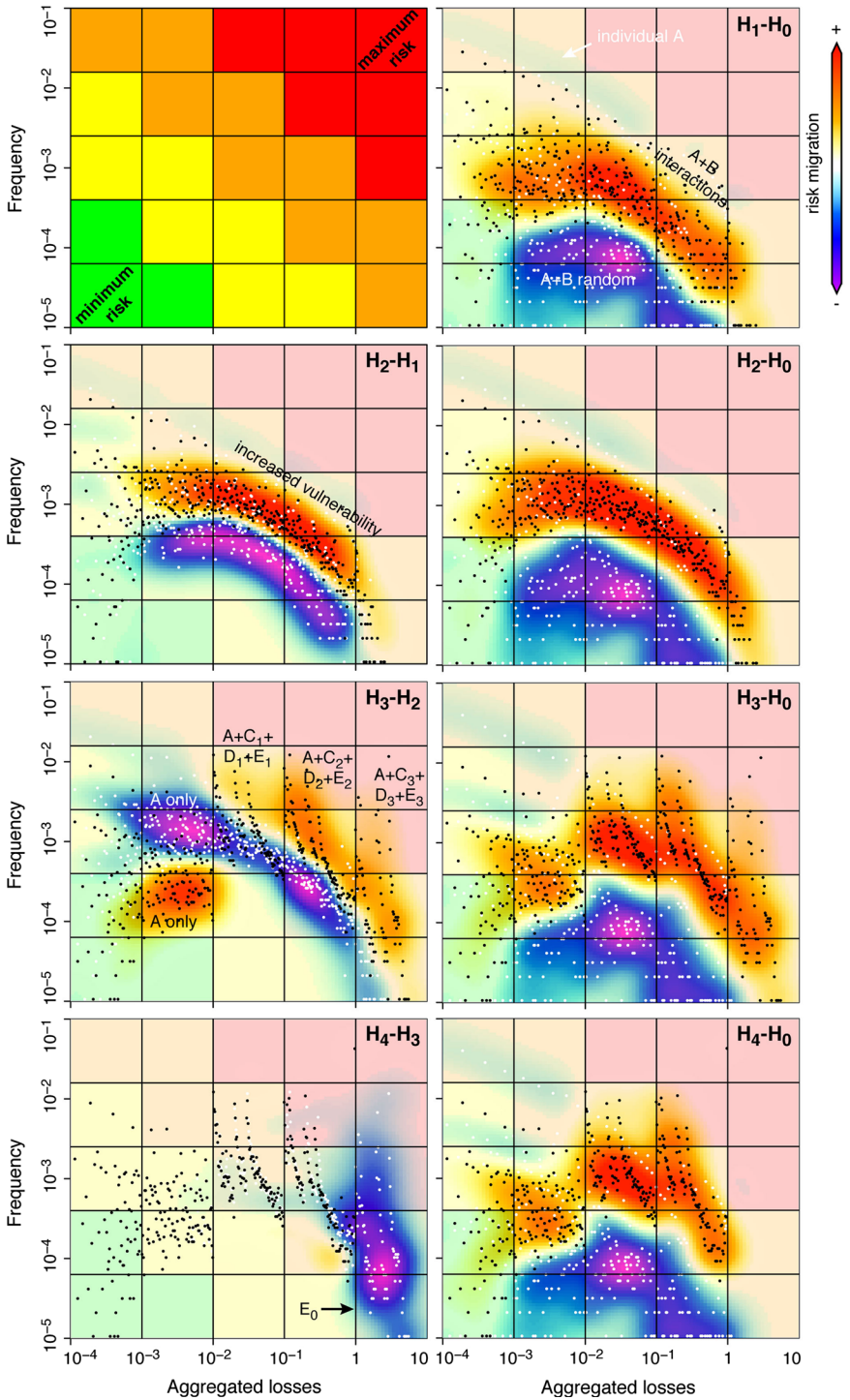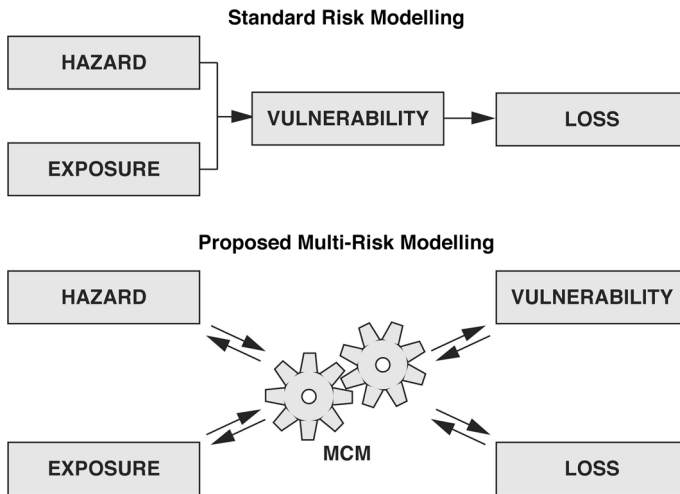
Fig. 12 Structure difference between standard risk modelling (following Grossi et al. 2005) and the newly proposed multi-risk approach. MCM refers to the sequential MCM defined in Sect. 2

Lagomarsino and Giovinazzi 2006). This second requirement is non-trivial, not only due to the different modelling structure, but also to the use here of a stochastic event set instead of aggregated hazard. Aggregated hazard is used for instance in standard seismic risk assessment (e.g., Cornell 1968) and in its recent multi-risk extensions (Marzocchi et al. 2012; Selva 2013). Nonetheless, moving to an event-based sequential simulation approach seems appropriate to model dynamic risk processes and extremes.

Testing of the proposed multi-risk framework has been made possible thanks to the heuristic method and the definition of generic perils and processes, which is based on the idea of "scientific imagination" (Kameda 2012; Paté-Cornell 2012). We have shown that the hazard correlation matrix, by adding knowledge of potential interaction processes, allows for the capture of low-probability–high-consequences events. In particular, we have shown the role of risk migration and of risk amplification for their occurrence. The present work should be seen as a proof-of-concept as we did not attend to fully resolve the difficult problem of extremes. We only considered a selected number of possible interactions, but while the chains of events that emerge in the system may seem obvious, adding more perils and more interactions will yield more complex risk patterns. We thus recommend a brick-by-brick approach to the modelling of multi-risk, to progressively reduce epistemic uncertainties. A more realistic modelling of low-probability–high-consequences events will also require the consideration of additional aspects, such as uncertainties (e.g., Barker and Haimes 2009), domino effects in socioeconomic networks (e.g., Adachi and Elling-wood 2008; Buldyrev et al. 2010) and long-term processes (Grossi and Kunreuther 2005; Smolka 2006), such as climate change (Garcin et al. 2008), infrastructure ageing (Rao et al. 2010) and exposure changes (Bilham 2009). While the concepts developed in the present study can suggest the theoretical benefits of multi-risk assessment, identifying their real-world practicality will require the application of the proposed framework to real test sites.

References

Adachi T, Ellingwood BR (2008) Serviceability of earthquake-damaged water systems: effects of electrical power availability and power backups systems on system vulnerability. Reliab Eng Syst Saf 93:78–88. doi:10.1016/j.ress.2006.10.014

Barker K, Haimes YY (2009) Assessing uncertainty in extreme events: applications to risk-based decision making in interdependent infrastructure sectors. Reliab Eng Syst Saf 94:819–829. doi:10.1016/j.ress.2008.09.008

Bier VM, Haimes YV, Lambert JH, Matalas NC, Zimmerman R (1999) A survey of approaches for assessing and managing the risk of extremes. Risk Anal 19:83–94

Bilham R (2009) The seismic future of cities. Bull Earthq Eng. doi:10.1007/s10518-009-9147-0

Brown P, Spalding RE, ReVelle DO, Tagliaferri E, Worden SP (2002) The flux of small near-Earth objects colliding with the Earth. Nature 420:294–296

Buldyrev SV, Parshani R, Paul G, Stanley HE, Havlin S (2010) Catastrophic cascade of failures in interdependent networks. Nature 464:1025–1028. doi:10.1038/nature08932

Carpignano A, Golia E, Di Mauro C, Bouchon S, Nordvik J-R (2009) A methodological approach for the definition of multi-risk maps at regional level: first application. J Risk Res 12:513–534. doi:10.1080/13669870903050269

Cornell C (1968) Engineering seismic risk analysis. Bull Seismol Soc Am 59:1583–1606

Cox T (1998) Risk integration and decision-making. In: Kirchssteiger C, Christou MD, Papadakis GA (eds) Risk assessment and management in the context of the Seveso II Directive. Industrial Safety Series, 6. Elsevier, Amsterdam

Eggert S, Walter TR (2009) Volcanic activity before and after large tectonic earthquakes: observations and statistical significance. Tectonophysics 471:14–26. doi:10.1016/j.tecto.2008.10.003

Fabbrocino G, Iervolino I, Orlando F, Salzano E (2005) Quantitative risk analysis of oil storage facilities in seismic areas. J Hazardous Mater A123:61–69. doi:10.1016/j.jhazmat.2005.04.015

Garcin M, Desprats JF, Fontaine M, Pedreros R, Attanayake N, Fernando S, Siriwardana CHER, De Silva U, Poisson B (2008) Integrated approach for coastal hazards and risks in Sri Lanka. Nat Hazards Earth Syst Sci 8:577–586

Gill JC, Malamud BD (2012) Reviewing and visualising interaction relationships for natural hazards, EGU General Assembly 2012, 22–27 April, 2012, Vienna, Austria, 708

Grossi P, Kunreuther H (eds) (2005) Catastrophe modeling: a new approach to managing risk. Springer, Berlin

Grossi P, Kunreuther H, Windeler D (2005) Chapter 2—an introduction to catastrophe models and insurance. In: Grossi P, Kunreuther H (eds) Catastrophe modeling: a new approach to managing risk. Springer, Berlin, pp 23–42

Grünthal G, Thieken AH, Scharz J, Radtke KS, Smolka A, Merz B (2006) Comparative risk assessments for the city of cologne—storms, floods, earthquakes. Nat Hazards 38:21–44. doi:10.1007/s11069-005-8598-0

Gutenberg B, Richter CF (1944) Frequency of earthquakes in California. Bull Seismol Soc Am 34:185–188

Hill DP, Pollitz F, Newhall C (2002) Earthquake–volcano interactions. Phys Today 55(11):41–47

Irish JL, Resio DT, Ratcliff JJ (2008) The influence of storm size on hurricane surge. J Phys Oceanogr 38:2003–2013. doi:10.1175/2008JPO3727.1

Jalayer F, Asprone D, Prota A, Manfredi G (2010) A decision support system for post-earthquake reliability asessment of structures subjected to aftershocks: an application to L'Aquila earthquake, 2009. Bull Earthq Eng. doi:10.1007/s10518-010-9230-6

Kameda H (2012), Engineering agenda on nuclear safety from the 2011 Tohoku-Pacific earthquake. In: Proceedings of international symposium engineering lessons learned from the 2011 great East Japan Earthquake, March 1–4, 2012, Tokyo, Japan, 102–121

Kappes MS, Keiler M, von Elverfeldt K, Glade T (2012) Challenges of analyzing multi-hazard risk: a review. Nat Hazards 64:1925–1958. doi:10.1007/s11069-012-0294-2

King GCP (2007) Fault interaction, earthquake stress changes, and the evolution of seismicity. In: Schubert G (ed) Treatise on geophysics, vol 4. Elsevier, Oxford, pp 225–256

Komendantova N, Mrzyglocki R, Mignan A, Khazai B, Wenzel F, Patt A, Fleming K (2014) Multi-hazard and multi-risk decision support tools as a part of participatory risk governance: Feedback from civil protection stakeholders. Int J Disaster Risk Reduct 8:50–67. doi:10.1016/j.ijdrr.2013.12.006

Krausmann E, Cozzani V, Salzano E, Renni E (2011) Industrial accidents triggered by natural hazards: an emerging risk issue. Nat Hazards Earth Syst Sci 11:921–929. doi:10.5194/nhess-11-921-2011

Lagomarsino S, Giovinazzi S (2006) Macroseismic and mechanical models for the vulnerability and damage assessment of current buildings. Bull Earthq Eng 4:415–443. doi:10.1007/s10518-006-9024-z

Mailier PJ, Stephenson DB, Ferro CAT, Hodges KI (2006) Serial clustering of extratropical cyclones. Mon Weather Rev 134:2224–2240

Marzocchi W, Garcia-Aristizabal A, Gasparini P, Mastellone ML, Di Ruocco A (2012), Basic principles of multi-risk assessment: a case study in Italy. Nat Hazards. doi:10.1007/s11069-012-0092-x

Mignan A, Grossi P, Muir-Wood R (2011) Risk assessment of Tunguska-type airbursts. Nat Hazards 56:869–880. doi:10.1007/s11069-010-9597-3

Parsons T (2005), Significance of stress transfer in time-dependent earthquake probability calculations. J Geophys Res 110:B05S02. doi:10.1029/2004JB003190

Paté-Cornell E (2012) On "Black Swans" and "Perfect Storms": risk analysis and management when statistics are not enough. Risk Anal 32:1823–1833. doi:10.1111/j.1539-6924.2011.01787.x

Piccardi L, Masse WB (eds) (2007) Myth and geology. Geological Society, London, Special Publications, 273

Rao AS, Lepech MD, Kiremidjian AS, Sun XY (2010) Time varying risk modeling of deteriorating bridge infrastructure for sustainable infrastructure design, 5th international conference on bridge maintenance safety management and life cycle optimization. CRC Press, Taylor & Francis Group, 2494–2501

Reese S, Ramsay D (2010) RiskScape: flood fragility methodology. NIWA Technical Report: WLG2010-45, p 46

Scheffers A, Scheffers S, Squire P (2012) Trimlines as evidence for palaeo-tsunamis. Nat Hazards 63:165–179. doi:10.1007/s11069-010-9691-6

Schmidt J, Matcham I, Reese S, King A, Bell R, Henderson R, Smart G, Cousins J, Smith W, Heron D (2011) Quantitative multi-risk analysis for natural hazards: a framework for multi-risk modelling. Nat Hazards 58:1169–1192. doi:10.1007/s11069-011-9721-z

Selva J (2013) Long-term multi-risk assessment: statistical treatment of interaction among risks. Hazards, Nat. doi:10.1007/s11069-013-0599-9

Simkin T, Siebert L (1994) Volcanoes of the world, 2nd edn. Geoscience Press, Tucson

Smolka A (2006) Natural disasters and the challenge of extreme events: risk management from an insurance perspective. Philos Trans R Soc A 364:2147–2165. doi:10.1098/rsta.2006.1818

Sornette D, Ouillon G (2012) Dragon-kings: mechanisms, statistical methods and empirical evidence. Eur Phys J Spec Top 205:1–26. doi:10.1140/epjst/e2012-01559-5

Spence RJS, Kelman I, Zuccaro PJ, Petrazzuoli S (2005) Residential building and occupant vulnerability to tephra fall. Nat Hazards Earth Syst Sci 5:477–494. doi:1684-9981/nhess/2005-5-477

Srivihok P, Honda K, Ruangrassamee A, Muangsin V, Naparat P, Foytong P, Promdumrong N, Aphimaeteethomrong P, Intavee A, Layug JE, Kosin T (2012) Development of an online tool for tsunami inundation simulation and tsunami loss estimation. Cont Shelf Res. doi:10.1016/j.csr.2012.08.021

Suppasri A, Imamura F, Koshimura S (2012) Tsunamigenic ratio of the Pacific Ocean earthquakes and a proposal for a Tsunami Index. Nat Hazards Earth Syst Sci 12:175–185. doi:10.5194/nhess-12-175-2012

Taleb NN (2007) The Black Swan: the impact of the highly improbable. Random House, New York

Toda S, Stein RS, Reasenberg PA, Dieterich JH, Yoshida A (1998) Stress transferred by the 1995 Mw = 6.9 Kobe, Japan, shock: effect on aftershocks and future earthquake probabilities. J Geophys Res 103(B10):24543–24565

Vitolo R, Stephenson DB, Cook IM, Mitchell-Wallace K (2009) Serial clustering of intense European storms. Meteorol Zeitschrift 18:411–424

Wehner M, Ginger J, Holmes J, Sandland C, Edwards M (2010) Development of methods for assessing the vulnerability of Australian residential building stock to severe wind, IOP Conf Ser Earth Environ Sci 11, doi:10.1088/1755-1315/11/1/012017

Zuccaro G, Cacace F, Spence RJS, Baxter PJ (2008) Impact of explosive eruption scenarios at Vesuvius. J Volcanol Geotherm Res 178:416–453. doi:10.1016/j.jvolgeores.2008.01.005